Computers & Fluids 50 (2011) 35–45

Contents lists available at ScienceDirect

Computers & Fluids

journal homepage: www.elsevier.com/locate/compfluid

Blending of miscible liquids with different densities starting from a stratified state

J.J. Derksen

Chemical & Materials Engineering, University of Alberta, Edmonton, Alberta, Canada T6G 2G6

ARTICLE INFO

Article history:
Received 7 May 2010
Received in revised form 6 May 2011
Accepted 23 June 2011
Available online 6 August 2011

Keywords:
Mixing
Blending
Buoyancy
Stratified liquids
Simulations
Turbulent flow
Active scalar

ABSTRACT

Homogenization of initially segregated and stably stratified systems consisting of two miscible liquids with different density and the same kinematic viscosity in an agitated tank was studied computationally. Reynolds numbers were in the range of 3000–12,000 so that it was possible to solve the flow equations without explicitly modeling turbulence. The Richardson number that characterizes buoyancy was varied between 0 and 1. The stratification clearly lengthens the homogenization process. Two flow regimes could be identified. At low Richardson numbers large, three-dimensional flow structures dominate mixing, as is the case in non-buoyant systems. At high Richardson numbers the interface between the two liquids largely stays intact. It rises due to turbulent erosion, gradually drawing down and mixing up the lighter liquid.

1. Introduction

Mixing in stratified fluids has received much attention in environmental fluid mechanics and related research areas [1–3]. Flows (partly) driven by buoyancy, or stabilized by density differences are abundant in oceans and the atmosphere. In oceans density differences are due to water streams having different salinity or temperature. Also in engineered systems homogenization of miscible liquids having different densities has relevant applications, e.g. in food processing and (petro)chemical industries. We expect an impact of the density differences and thus buoyancy on the homogenization process. In this paper we focus on mixing starting from stable stratifications, i.e. mixing starting from an initial situation where a lighter liquid sits on top of a denser liquid. When agitated (e.g. by an impeller), vertical mixing in such stratifications is an energy sink, in addition to the viscous dissipation occurring in the liquid. We also anticipate the (turbulent) flow structures to be influenced by buoyancy forces [4].

In engineering-mixing and agitated flow research, blending, homogenization, scalar mixing, and determination of mixing times are extensively studied topics with an abundance of papers (discussing experimental and computational procedures and results). The impact of density differences and stratification on the blending process in agitated tanks is a subject less frequently encountered in the literature. A part of the extensive (and classical) set of experiments on agitation of miscible liquids reported by van de Vusse [5] was done starting from stable stratifications. Further experimental work in the field is due to Ahmad et al. [6] and Rielly and Pandit [7]. Bouwmans et al. [8] visualized mixing of small additions of liquid having a density different from the bulk density. The author is not aware of computational studies of blending through agitation in stably stratified liquids.

The specific situation that is considered in this paper is a conceptually simple one. Two miscible liquids (one heavy, one light) are placed in a mixing tank. The light liquid occupies the upper part of the volume, the heavy liquid the lower part, the interface being at half the tank height. Since we focus on the impact of density differences and to limit the dimensionality of the parameter space, the two liquids are given the same kinematic viscosity. The tank is equipped with a mainly axially (=vertically in this case) pumping impeller: a 45° pitched-blade turbine having four blades. Baffles at the perimeter of the cylindrical tank wall prevent the liquid in the tank from largely rotating as a solid body. At time zero – when the velocity is zero everywhere in this stable system – the impeller starts to rotate with a constant angular velocity and the blending process starts.

Given the tank and impeller geometry, the fact that the top of the tank is closed-off with a lid, and given the initial conditions, two dimensionless numbers govern the flow dynamics: a Reynolds number (Re) and a Richardson number (Ri), the latter being a measure for the ratio of buoyancy forces over inertial forces. In this paper we explore this two-dimensional parameter space by means of numerical simulations: we solve the flow equations and in addition solve for the transport equation of a scalar that represents the local composition of the liquid in the tank. This composition is fed

E-mail address: jos@ualberta.ca

0045-7930/$ - see front matter © 2011 Elsevier Ltd. All rights reserved.
doi:10.1016/j.compfluid.2011.06.013

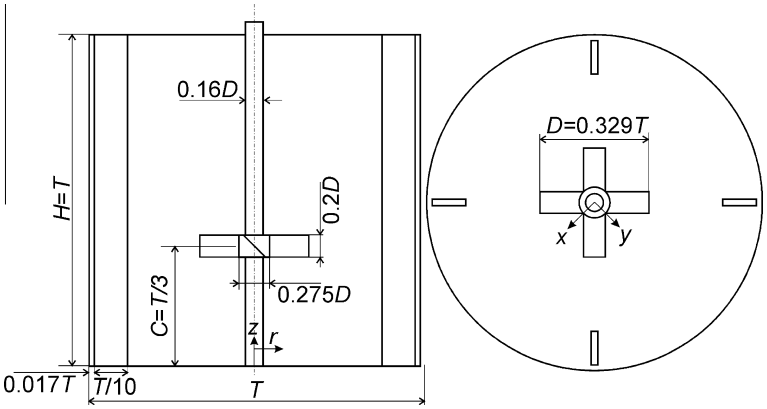

Fig. 1. The stirred tank geometry considered in this paper. Baffled tank with pitched-blade impeller. The coordinate systems ((r, z) and (x, y, z)) are fixed and have their origin in the center at the bottom of the tank. The top of the tank is closed off with a lid.

back to the flow dynamics in terms of a buoyancy force (active scalar). We study the way the homogenization process evolves in time in terms of the flow field and the density distributions in the tank as a function of Re and Ri. This eventually leads to quantitative information as to what extent the process (i.e. homogenization) times are influenced by stabilization as a result of buoyancy forces.

The Reynolds numbers are chosen such that they allow for direct simulations of the flow, i.e. we do not employ closure relations for turbulent stresses or subgrid-scale stress models. On the one hand this limits the range of Reynolds numbers that can be studied; on the other hand it allows us to fully focus on the flow physics without interference of potential artifacts or speculative issues associated with turbulence modeling in the presence of buoyancy.

The research discussed here is purely computational. The results, however, are very amenable to experimental verification, and next to quantitatively describing mixing in the presence of buoyancy the aim of this paper is to trigger experimental work on flow systems similar (not necessarily identical) to the ones studied here. In this respect: the choice in this study of giving the liquids the same kinematic viscosity is not instigated by limitations of the numerical method; in fact our method can very well deal with variable viscosity flows [9]. Combined experimental and computational research could eventually lead to improved equipment designs for mixing tasks involving stratification.

The paper is organized in the following manner: First the flow system is described, and dimensionless numbers are defined. Subsequently the simulation procedure is discussed. We then present results, first showing qualitative differences in mixing at different Richardson (and Reynolds) numbers, then quantifying the homogenization process. Conclusions are summarized in the last section.

2. Flow system

The tank and agitator, and the coordinate system as used throughout this work are shown in Fig. 1. The tank is cylindrical with four equally spaced baffles along the perimeter. The flow is driven by four pitched (45°) blades attached to a hub that is mounted on a shaft that runs over the entire height of the tank. The tank is closed off with a lid so that at the top surface (as on all other solid surfaces) a no-slip condition applies. The Reynolds number of this flow system is defined as $\mathrm{Re} = \frac{ND^2}{\nu}$, with N the impeller speed (in rev/s), D the impeller diameter (see Fig. 1) and the ν kinematic viscosity of the liquid which is uniform throughout the tank, i.e. ν is independent of the local composition of the liquid.

Initially, two layers of liquid are placed in the tank, their interface being at $z = 0.5H$. The upper liquid has a density that is $\Delta\rho$ less than that of the lower liquid. The volume of the denser liquid is less by the volume of the impeller compared to the volume of lighter liquid. Starting from a completely still situation, we switch on the impeller with constant speed N. Next to the Reynolds number, a Richardson number defined as $\mathrm{Ri} = \frac{g\Delta\rho}{\rho N^2 D}$ now fully pins down the flow system. In the expression for Ri, g is gravitational acceleration, and ρ is the volume-averaged density of the liquid in the tank. Rielly and Pandit [7] define the Richardson number as $\frac{g\Delta\rho H}{\rho N^2 D^2}$. Given the (standard) aspect ratios as used in the present work the latter expression is equal to three times the Richardson number as we defined it above.

The Reynolds numbers considered are in the range of 3000–12,000. For a single-liquid system this range covers transitional and mildly turbulent flow. The Richardson number ranges from 0.0 to 1.0.

3. Modeling approach

The lattice-Boltzmann method (LBM) has been applied to numerically solve the incompressible flow equations. The method originates from the lattice-gas automaton concept as conceived by Frisch, Hasslacher, and Pomeau in 1986 [10]. Lattice gases and lattice-Boltzmann fluids can be viewed as (fictitious) fluid particles moving over a regular lattice, and interacting with one another at lattice sites. These interactions (collisions) give rise to viscous behavior of the fluid, just as colliding/interacting molecules do in real fluids. Since 1987 particle-based methods for mimicking fluid flow have evolved strongly, as can be witnessed from review articles and text books [11–14]. The main reasons for employing the LBM for fluid flow simulations are its computational efficiency and its inherent parallelism, both not being hampered by geometrical complexity.

In this paper the LBM formulation of Somers [15] has been employed. It falls in the category of three-dimensional, 18 speed (D3Q18) models. Its grid is uniform and cubic. Planar, no-slip walls naturally follow when applying the bounce-back condition. For non-planar and/or moving walls (that we have in case we are simulating the flow in a cylindrical, baffled mixing tank with a revolving impeller) an adaptive force field technique (a.k.a. immersed boundary method) has been used [16,17].

The local composition of the liquid is represented by a scalar field c for which we solve a transport equation

$$\frac{\partial c}{\partial t} + u_i \frac{\partial c}{\partial x_i} = \Gamma \frac{\partial^2 c}{\partial x_i^2} \tag{1}$$

(summation over repeated indices) with u_i the ith component of the fluid velocity vector, and Γ a diffusion coefficient that follows from setting the Schmidt number $\mathrm{Sc} \equiv \frac{\nu}{\Gamma}$ to 1000. We solve

Eq. (1) with an explicit finite volume discretization on the same (uniform and cubic) grid as the LBM. A clear advantage of employing a finite volume formulation is the availability of methods for suppressing numerical diffusion. As in previous works [18,19], TVD discretization with the Superbee flux limiter for the convective fluxes [20] was employed. We step in time according to an Euler explicit scheme. This explicit finite volume formulation for scalar transport does not hamper the parallelism of the overall numerical approach.

Strictly speaking the Schmidt number is the third dimensionless number (next to Re and Ri) defining the flow. Its large value (10^3) makes the micro-scalar-scales (Batchelor scale) a factor of $\sqrt{\mathrm{Sc}} \approx 30$ smaller than the Kolmogorov length scale and quite impossible to resolve in our numerical simulations. In the simulations – although we as much as possible suppress numerical diffusion – diffusion will be controlled by the grid spacing and the precise value of Sc based on molecular diffusivity will have marginal impact on the computational results. In order to assess to what extent numerical diffusion influences the outcomes of our simulations we performed a grid refinement study for a few of the flow cases considered here.

The scalar concentration c is coupled to the flow field via a Boussinesq approximation. The concentration is used to determine a local mixture density ρ_{mx} according to a linear relation: $\rho_{mx} = \rho + (\frac{1}{2} - c)\Delta\rho$ ($c = 1$ light fluid; $c = 0$ heavy fluid). The body force in positive z-direction (see Fig. 1) felt by a liquid element having density ρ_{mx} then is equal to

$$f_z = g(\rho - \rho_{mx}) = g\Delta\rho\left(c - \frac{1}{2}\right) \tag{2}$$

and this force is incorporated in the LB scheme. Since the volume of the light fluid is a little larger than the volume of heavy fluid (by the volume of the impeller), the uniform concentration after sufficiently long mixing is $c_\infty = 0.502$ (not exactly 0.50). This leaves us with a small, uniform buoyancy force in the fully mixed state. This uniform force, however, has no impact on the flow dynamics; its only consequence is a hydrostatic pressure gradient. This was tested by running a simulation with $f_z = g\Delta\rho c$ (instead of Eq. (2)) so that the eventual uniform buoyance force got $f_z = 0.502g\Delta\rho$. The flow dynamics of the latter simulation was the same as that of the corresponding simulation that used Eq. (2).

In the Boussinesq approximation, the body force term is the only place where the density variation enters the Navier–Stokes equations. For this approximation to be valid $\frac{\Delta\rho}{\rho} \ll 1$, (that is $\mathrm{Ri} \ll \frac{g}{N^2 D}$) is required.

3.1. Numerical settings

The default grid (which as explained above is uniform and cubic) has a spacing Δ such that 180Δ corresponds to the tank diameter T (defined in Fig. 1). The number of time steps to complete one impeller revolution is 2000. In this manner the tip speed of the impeller is $\pi ND = 0.094$ in lattice units (with the impeller diameter $D = T/3$) which keeps the flow velocities in the tank well below the

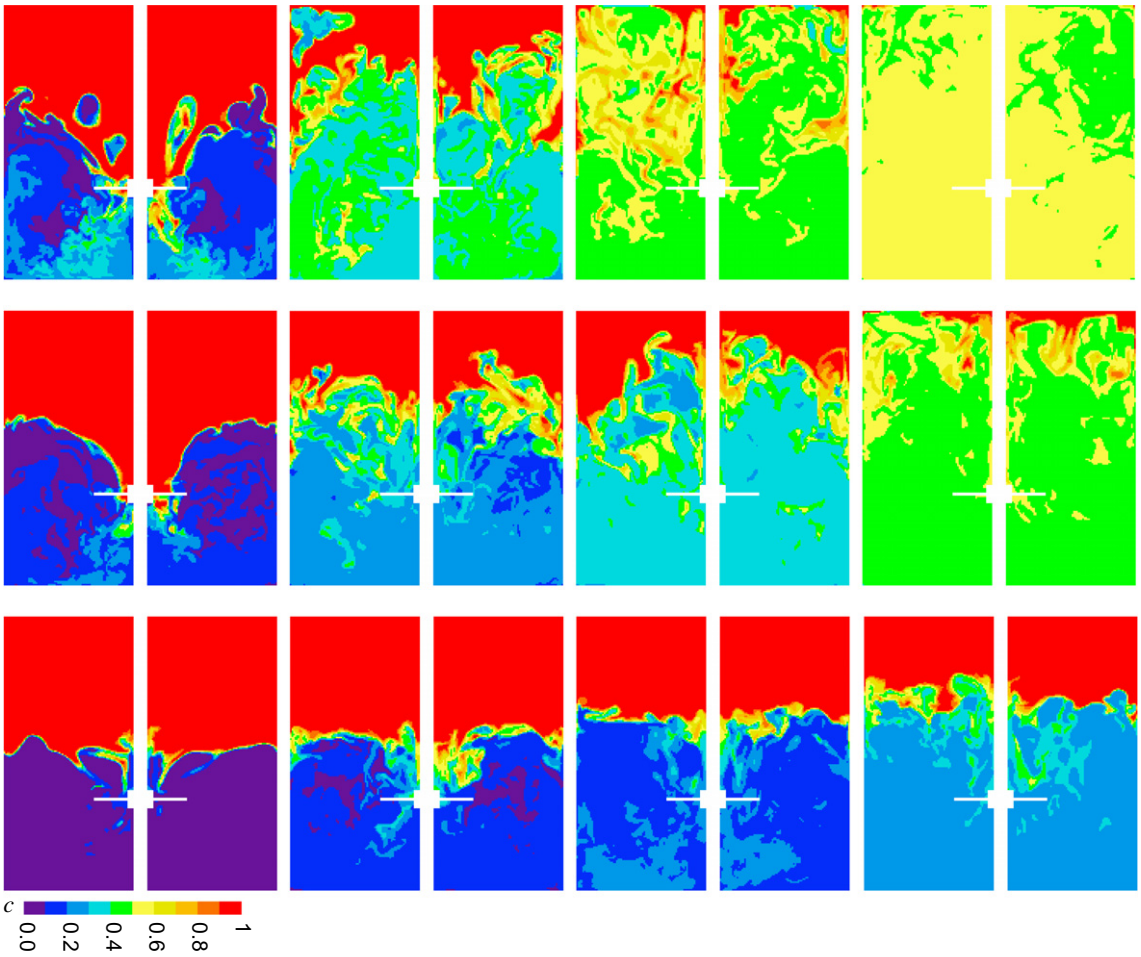

Fig. 2. Liquid composition c in a vertical, mid-baffle plane at (from left to right) 10, 20, 30, and 50 impeller revolutions after start up. From top to bottom Ri = 0.0, 0.125, and 0.5. Re = 6000. (For interpretation to colours in this figure, the reader is referred to the web version of this paper.)

speed of sound of the lattice-Boltzmann system thus achieving incompressible flow.

The effect of the spatial resolution of the simulations on the flow results needs to be examined. The micro-scale of turbulence (Kolmogorov length scale η) relates to a macroscopic length scale (say the tank diameter T) according to $\eta = T\mathrm{Re}^{-\frac{3}{4}}$. The criterion for sufficiently resolved direct numerical simulations of turbulence is $\Delta < \pi\eta$ [21,22]. According to this criterion, at Re = 6000 a grid with $T = 180\Delta$ slightly under-resolves the flow; at our highest Reynolds number (Re = 12,000) the same grid has $\Delta \approx 6.4\eta$. To assess how serious this apparent lack of resolution is, grid effects were investigated. In addition to $T = 180\Delta$, a number of simulations have also been performed on grids with $T = 240\Delta$. One simulation with Re = 12,000 used a grid with $T = 330\Delta$ (so that for this simulation $\Delta \approx 3.5\eta$). Due to the explicit nature of the lattice-Boltzmann method and its (in)compressibility constraints, the finer grids require more time steps per impeller revolution.

The relatively modest default resolution of $T = 180\Delta$ was chosen because scanning the two-dimensional parameter space (Re and Ri) requires a significant number of simulations, and since the simulations need to capture at least the largest part of the homogenization process, i.e. the evolution from a segregated, static state to a well-mixed, dynamic state. Dependent on Re and Ri, the time span per simulation varied from 100 to slightly over 200 impeller revolutions.

4. Results

4.1. Flow and scalar field impressions

The results of our simulations will be mostly discussed in terms of the flow and concentration fields in the vertical, mid-baffle cross section as they evolve in time from start-up from a zero-flow, fully segregated, stable state. The base-Reynolds number amounts to 6000. For this value of Re we show in Fig. 2 the scalar concentration fields for three different values of Ri, one of them being a non-buoyant, and thus passive-scalar case (Ri = 0.0). Buoyancy clearly impacts the mixing process. At Ri = 0.0 the interface between high and low concentration quickly disintegrates and e.g. low-concentration blobs appear in the high-concentration upper portion of the cross section as a results of three-dimensional flow effects, largely due to the presence of baffles. At Ri = 0.125 this is less the case. The interface is clearly agitated but largely keeps its integrity, i.e. it is not broken up. At still larger Ri (Ri = 0.5 in Fig. 2) the interface stays more or less horizontal. It rises as a result of erosion: High-concentration (and thus low-density) liquid is eroded from the interface and drawn down to the impeller. It then quickly mixes in the lower part of the tank. This leads to a gradual rise of concentration in the part of the tank underneath the interface. The portion above the interface stays at concentration one and gradually reduces in height.

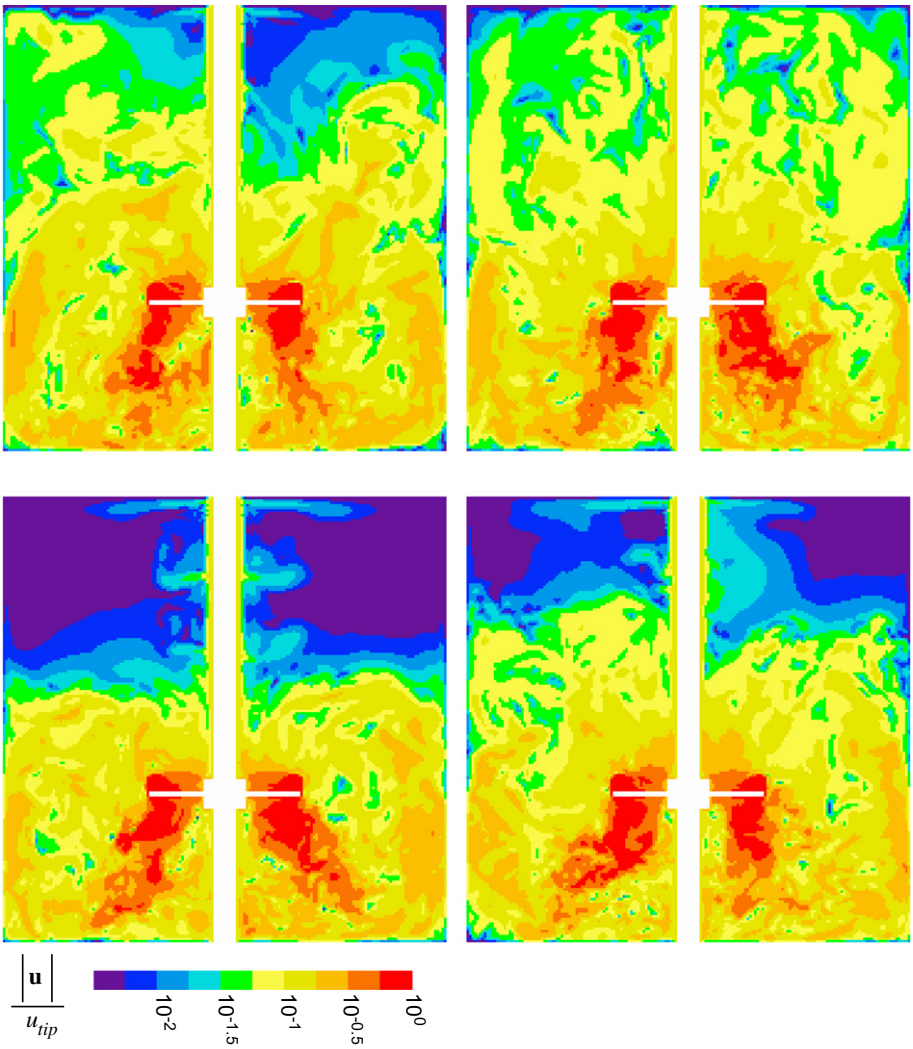

Fig. 3. Velocity magnitude in a mid-baffle plane. Top: Ri = 0.0; bottom Ri = 0.5. Left: 20 impeller revolutions after start-up, right: 50 revolutions after start up. Note the logarithmic color scale. (For interpretation of the references to color in this figure legend, the reader is referred to the web version of this article.)

After start up it takes time for the action of the impeller to be felt throughout the tank with the top of the tank the last region that gets agitated. In the absence of buoyancy the flow and turbulence induced by the impeller have made their way to the upper parts of the tank in roughly 30 impeller revolutions. At Ri = 0.5, the interface between high and low-density liquid acts as a barrier for flow development in the upper, low-density part of the tank, see Fig. 3. After 50 revolutions, high up in the tank there still exists a rather quiescent flow region where agitation is largely due to the rotation of the shaft, not so much the result of the impeller.

Compared to the impact the Richardson number has, the effect of the Reynolds number is relatively modest, as can be assessed from Fig. 4. Here we compare – at Ri = 0.125 – the scalar concentration fields in the mid-baffle plane at Re = 3000, and Re = 12,000 at two moments in time. These fields have their Re = 6000 counterparts displayed in Fig. 2 (middle row, second and fourth panel counted from the left). At the three Reynolds numbers, the interface reaches a level of $z \approx 2.2D$ after 20 revolutions, and is closely underneath the lid after 50 revolutions.

4.2. Quantitative analysis

The above impressions are now analyzed and interpreted in a more quantitative manner. One way to show the evolution of the mixing process is by means of vertical concentration profiles. These are cross-sectional averaged and time-smoothed profiles. The vertical concentration profile in the mid-baffle plane (with $y = 0$, see Fig. 1) is defined as $\tilde{c}(z,t) = \frac{1}{T}\int_{-T/2}^{T/2} c(x, y = 0, z, t)dx$. As the averaging time we take five impeller revolutions: $\langle\tilde{c}\rangle(z,t) = \frac{N}{5}\int_{t-\frac{2.5}{N}}^{t+\frac{2.5}{N}} \tilde{c}(z,\tau)d\tau$. In Fig. 5 the results with the three Reynolds numbers at Ri = 0.125 as above discussed in a qualitative manner are compared in terms of $\langle\tilde{c}\rangle$. Now we also get a clearer picture of the effect the Reynolds number has on the level of homogenization. Initially the three flow systems evolve at comparable pace (in line with the observations in Figs. 2 and 4); after 100 impeller revolutions, however, the systems with Re = 6000 and 12,000 are (virtually) vertically homogeneous, whereas at this stage the system with Re = 3000 still has appreciably higher concentrations in the top 10–20% of the tank volume, i.e. above $z = 0.8H$.

In Fig. 6 the impact of the Richardson number on the evolution of $\langle\tilde{c}\rangle$ at the base-case Reynolds number (Re = 6000) is presented. The results confirm the earlier qualitative observations. The profiles for Ri $\geqslant$ 0.25 show a fairly narrow range where the scalar concentration transits from a relatively low value in the bottom region, to $c = 1$ in the top region. This narrow range represents the interface; it slowly rises with time. Below the interface the scalar concentration is quite uniform and gradually increases as a result of turbulence attacking (eroding) the interface from below, and the impeller effectively spreading the eroded scalar through the portion of the tank below the interface. For Ri $\leqslant$ 0.125 the interface gets wider and less well-defined.

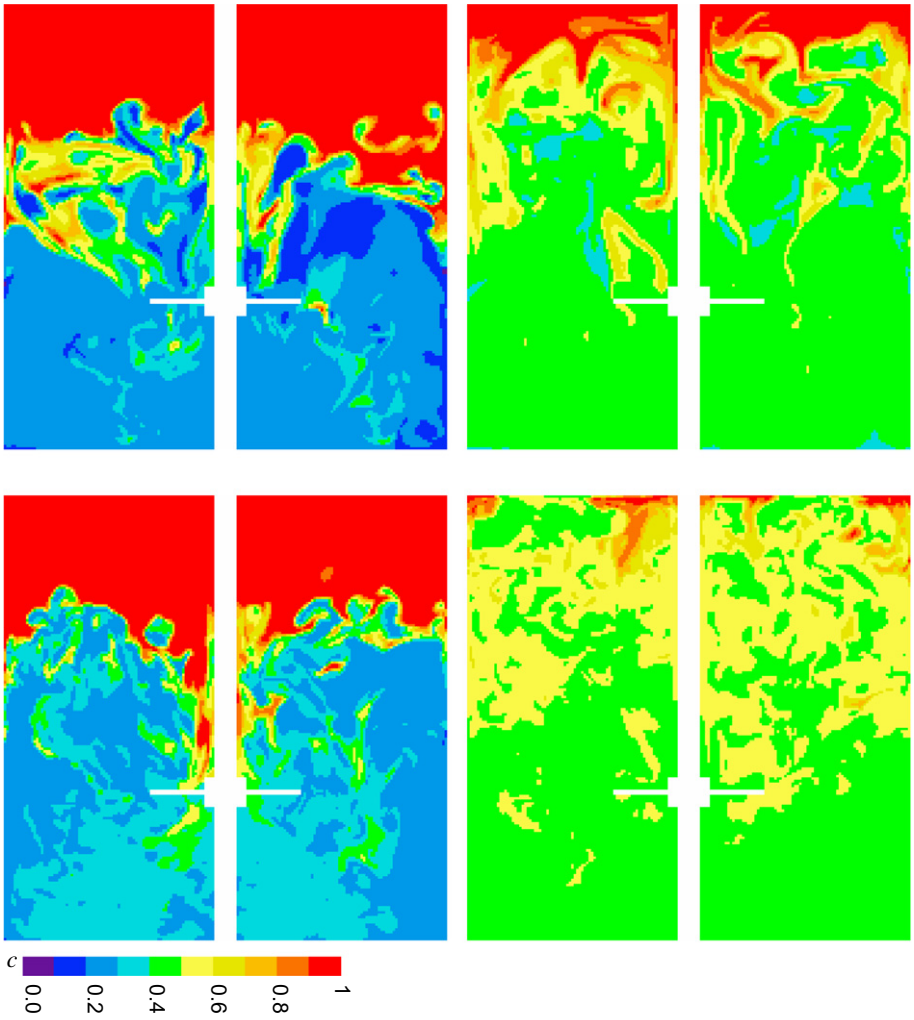

Fig. 4. Assessment of Reynolds number effects at Ri = 0.125. Top row: Re = 3000; bottom row: Re = 12,000 20 (left) and 50 (right) impeller revolutions after start up. (For interpretation to colours in this figure, the reader is referred to the web version of this paper.)

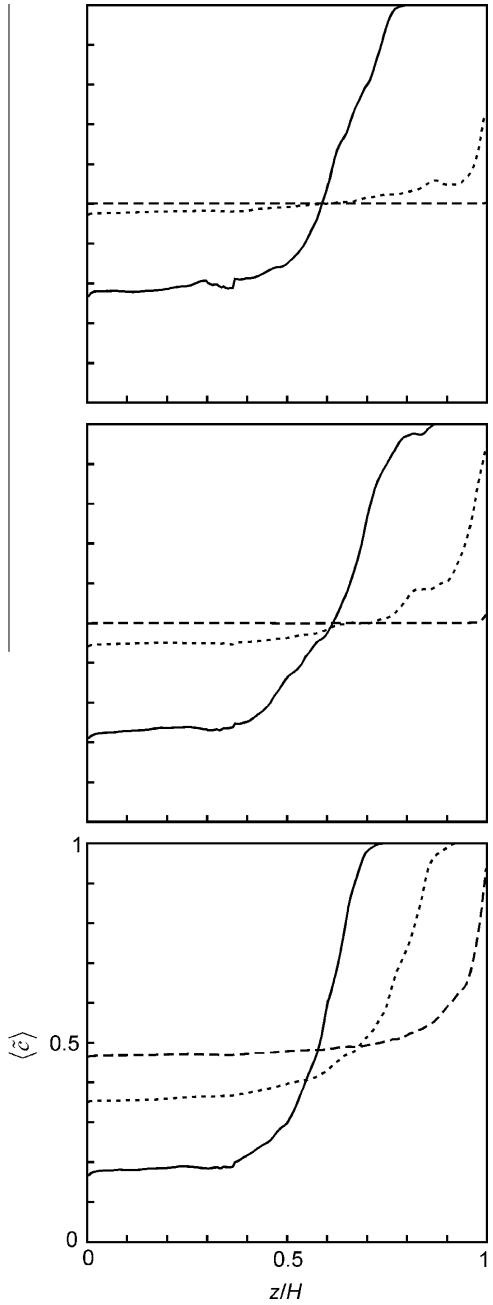

Fig. 5. Vertical concentration profiles $\langle\bar{c}\rangle$ (as defined in the text). The three curves per panel relate to $t = 17.5/N$ (time averaging from $15/N$ to $20/N$) (solid line), $t = 47.5/N$ (dotted line), and $t = 97.5/N$ (dashed line). From bottom to top: Re = 3000; 6000; and 12,000. Ri = 0.125.

The interface rising toward the top of the tank is again visualized in Fig. 7, where we track the interface location z_i (quite arbitrarily defined as the vertical (z) location with $\langle\bar{c}\rangle = 0.5$) as a function of time. For all Reynolds numbers considered the rising interface can be consistently tracked for Ri = 1.0 and Ri = 0.5. Also for Re = 3000 (the lowest Reynolds number considered) and Ri = 0.25 the interface rises coherently. For higher Reynolds numbers the interface evolves more irregularly and at some stage becomes intractable. The same is true if Ri < 0.25 (not shown in Fig. 7).

If possible (based on the level of coherency of the z_i versus time data) we define the interface rise velocity v_i as the slope of a linear function with intercept $z_i = 0.5$ at $t = 0$, and least-squares fitted through the z_i data points in the time range 0–100 impeller revolutions. This rise velocity as a function of Ri at the three Reynolds numbers is plotted in Fig. 8. It shows a consistent decrease of the rise velocity with increasing Richardson number. The (limited amount of) data points also show an increasing rise velocity with increasing Reynolds number. This is because the stronger turbulence at higher Re more effectively erodes the interface which is the primary reason for it to rise. The rise velocity can be used as a means to estimate the mixing time: $\tau_{mi} \approx \frac{0.5H}{v_i}$ with $0.5H$ the distance the interface needs to travel to reach the top of the tank.

In order to assess the effect of buoyancy on mixing for the cases without clearly identifiable interface rise velocity (notably the cases with Ri $\leqslant$ 0.25) we also analyzed the mid-baffle scalar concentration fields in terms of their spatial concentration standard deviation as a function of time: $\sigma^2(t) = \frac{1}{A}\iint_A [c^2(x, y = 0, z, t) - (\langle c\rangle(t))^2]dxdz$ with $\langle c\rangle(t)$ the average scalar concentration in the mid-baffle plane at moment t.

Time series of standard deviations are given in Fig. 9 for Re = 6000 and various Richardson numbers. The decay rates strongly depend on the Richardson number; at Ri = 0.03125 the scalar variance decay is close to that of a passive scalar so that we can conclude that (for the specific stirred tank configuration and process conditions) buoyancy influences the homogenization process if Ri > 0.03125. In order to characterize the decay of scalar variance with a single number, the time to reach $2\sigma = 0.05$ is here chosen as the mixing time measure τ_σ. If $2\sigma = 0.05$ the scalar concentration in the mid-baffle cross section is fairly uniform with only small high-concentration patched near the very top of the tank (see the inset in Fig. 9).

In Fig. 10 it is shown how the dimensionless mixing time $\tau_\sigma N$ relates to Ri and Re: the higher Ri, the larger the mixing time; the larger Re the lower the mixing time. For Ri = 0.0 (i.e. no buoyancy) correlations for mixing times based on experimental data are available. Grenville et al. [23] suggest $\tau_\sigma N = 5.1(\mathrm{Po})^{\frac{1}{3}}\left(\frac{T}{D}\right)^2$ with Po the power number (which is the power P drawn by the impeller made dimensionless according to $\mathrm{Po} \equiv \frac{P}{\rho D^5 N^3}$). With Po $\approx$ 1.2 for a four-blade 45° pitched-blade turbine [24] and $\frac{T}{D} \approx 3$ (see Fig. 1) the correlation gives $\tau_\sigma N \approx 43$ which is close to the results we present in Fig. 10 for Ri = 0.0.

Buoyancy amplifies the differences in mixing times between the various Reynolds numbers: at Ri = 0.0 the mixing times of the three Reynolds numbers are within 25%. By Ri = 0.0625 this has grown to some 50% and differences increase further for higher Ri. Specifically homogenization at the lowest Reynolds number (3000) slows down drastically. At this value the stratification makes it hard to sustain turbulence, specifically in the higher levels of the tank. Reduced fluctuation levels also have negative impact on the interface erosion process that – as discussed above – becomes more and more rate determining at higher Richardson numbers.

4.3. Assessment of grid effects

At this stage it is important to (again) realize that the results and their analysis presented so far is a purely computational exercise and that we have no experimental validation. In order to assess the quality of the results to some extent we here present their sensitivity with respect to the spatial and temporal resolution of the simulations: Three of the cases as discussed above were repeated on a grid with $\Delta = T/240$ and $\Delta t = 1/(2800N)$ (as discussed above the default values are $\Delta = T/180$ and $\Delta t = 1/(2000N)$). The three cases have (1) Re = 6000 and Ri = 0.25; (2) Re = 3000 and Ri = 1.0; (3) Re = 12,000 and Ri = 0.0625. In addition and given its high Reynolds number, the third case was also simulated on a grid with $\Delta = T/330$ and $\Delta t = 1/(3600N)$. We analyze these cases in the same way as their lower resolution counterparts. For the cases with Ri = 1.0 and 0.25 we determine their vertical, time-smoothed

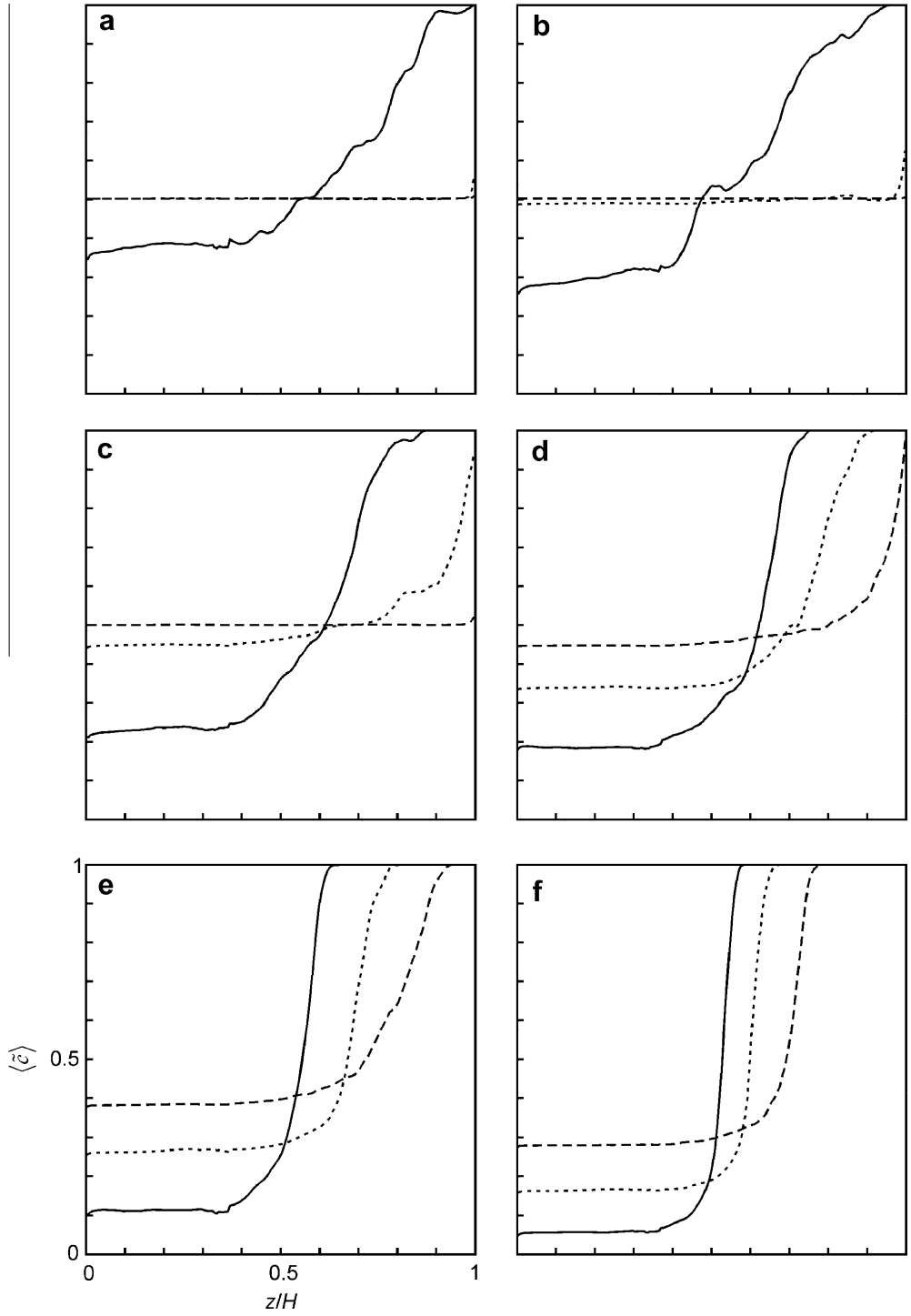

Fig. 6. Vertical concentration profiles $\langle \tilde{c} \rangle$ (as defined in the text). The three curves per panel relate to $t = 17.5/N$ (solid line), $t = 47.5/N$ (dotted line), and $t = 97.5/N$ (dashed line). All panels have Re = 6000, and (a) Ri = 0.0; (b) Ri = 0.0625; (c) Ri = 0.125; (d) Ri = 0.25; (e) Ri = 0.5; (f) Ri = 1.0.

concentration profiles, and track the rise of the interface. The case with Ri = 0.0625 is analyzed in terms of the decay of the scalar standard deviation with time, and in terms of its flow characteristics. The results are in Figs. 11–15.

In general there only is a weak sensitivity with respect to the grid size; the sensitivity getting stronger for higher Re. It can be seen (Fig. 11) that the concentration profiles at Re = 3000 agree better between the grids than the profiles at Re = 6000. Interpreting the concentration profiles in terms of the rise of the interface (Fig. 12) shows insignificant differences; the statistical uncertainties stemming from turbulence are at least as big as potential grid effects.

The test at Re = 12,000 and Ri = 0.0625 is more critical. It shows (in Fig. 13) a clear, and to be expected trend with respect to the grid resolution. Since diffusion is largely controlled by the numerics, the simulation on the finest grid is less diffusive and thus shows higher scalar standard deviations in the later stages of homogenization. The differences are not very large; the τ_σ mixing

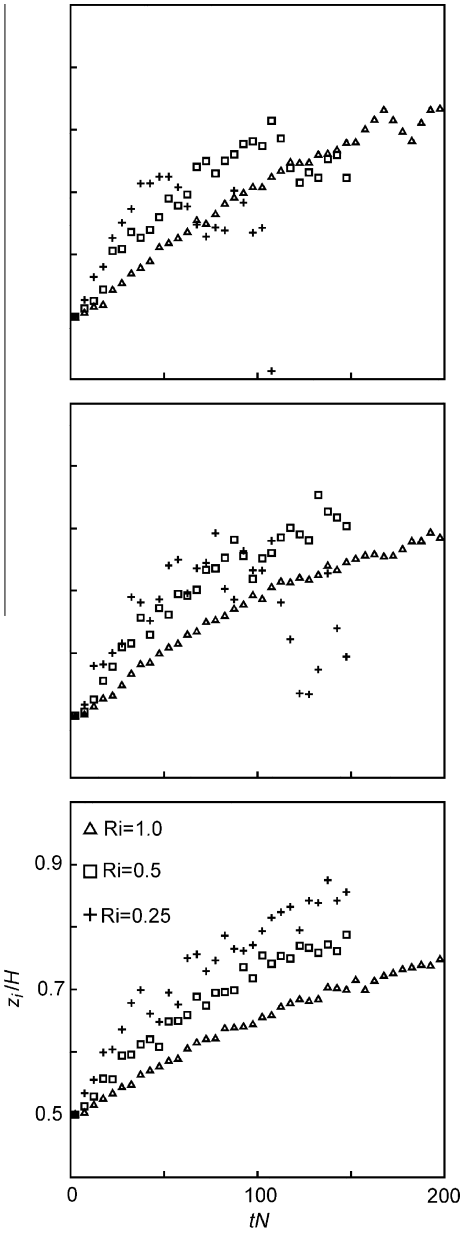

Fig. 7. Vertical interface location z_i as a function of time for (from bottom to top) Re = 3000; Re = 6000; and Re = 12,000; and Ri as indicated.

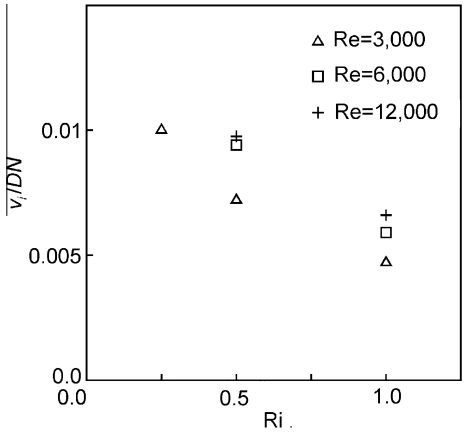

Fig. 8. Rise velocity of the interface as a function of Ri at various Reynolds numbers. Data points are only given when a coherent rising motion if the interface for at least $0 \leqslant tN \leqslant 100$ could be identified in time series as presented in Fig. 7.

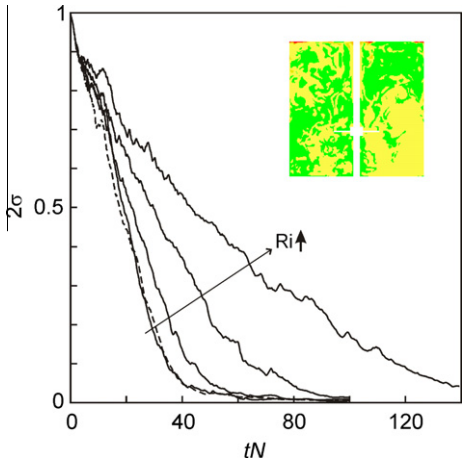

Fig. 9. Scalar standard deviation in the mid-baffle plane (σ) as a function of time; comparison of different Richardson numbers at Re = 6000. The dashed curve has Ri = 0.0. The solid curves have Ri = 0.03125, 0.0625, 0.125, and 0.25 in the order as indicated. The inset is the scalar field for Ri = 0.0 when $2\sigma = 0.05$ (at $tN = 40$). The color scale of the inset is the same as in Fig. 2. (For interpretation of the references to colours in this figure legend, the reader is referred to the web version of this paper.)

time increases by some 6% from the coarsest to the finest grid. It is believed that the essential flow physics is sufficiently captured by the default (and coarsest) grid.

In addition to the mixing time results, this is further assessed by comparing some important flow characteristics for the case with Re = 12,000 and Ri = 0.0625 on the three grids. The turbulent flow in the mixing tank is largely driven by the vortex structure around the impeller. In Fig. 14 we visualize this structure by plotting the vorticity-component in the direction normal to the mid-baffle plane. This view allows us to clearly see the strong vortices at the tips of the impeller blades, and the way they are advected in the downward direction by the pumping action of the impeller [25]. The data in Fig. 14 (and also in Fig. 15) have been averaged over the final 30 impeller revolutions during which the flow can be considered fully developed and stationary (the scalar is well mixed during this stage). The averaging is conditioned with the impeller angle (impeller-angle-resolved averages).

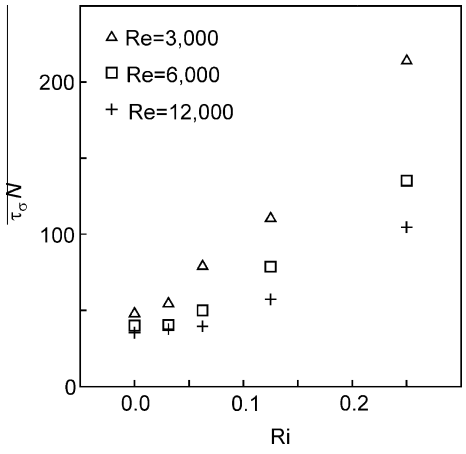

Fig. 10. The mixing time based on scalar standard deviation τ_σ versus Ri.

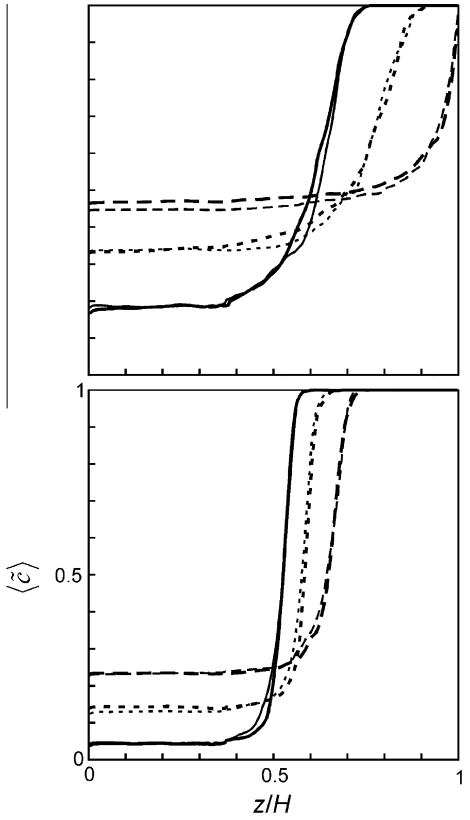

Fig. 11. Vertical concentration profiles $\langle \tilde{c} \rangle$. Comparison of simulations with different resolution. Top panel: Re = 6000, Ri = 0.25; bottom panel: Re = 3000, Ri = 1.0. The solid curves are at $t = 17.5/N$, the dotted curves at $t = 47.5/N$, and the dashed curves at $t = 97.5/N$. The thicker curves relate to the finer grid ($\Delta = T/240$), the thinner curves to the coarser (default) grid ($\Delta = T/180$).

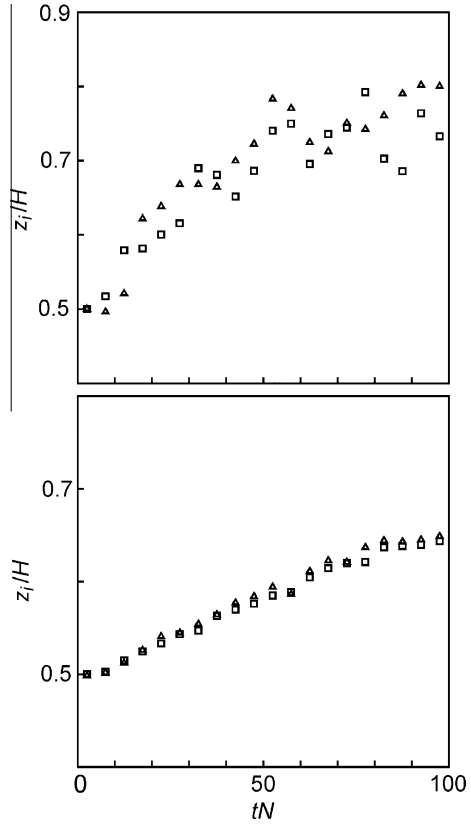

Fig. 12. Interface location z_i as a function of time; comparison between different grids; triangles relate to the finer grid, ($\Delta = T/240$), squares to the coarser (default) grid ($\Delta = T/180$). Top panel: Re = 6000, Ri = 0.25; bottom panel: Re = 3000, Ri = 1.0.

The vorticity levels of the tip vortices and their locations agree well between the three grids. More subtle differences between the grids can be observed as well: the decay of vorticity (i.e. its dissipation) along the downward and subsequently sideways directed impeller stream is stronger for the courser grids. Also the boundary layers (most clearly visible above the bottom and along the lower part of the tank's side wall) are better resolved by the finer grid, i.e. they show slightly higher vorticity levels. These effects of resolution were to be expected. They, however, do not strongly impact the overall flow in the tank which confirms the conclusions regarding the weak impact of resolution on mixing time as discussed above and presented in Fig. 13.

In Fig. 15 we compare impeller-angle resolved (with the impeller blades crossing the field of view) turbulent kinetic energy between the three grids. Again we see fairly good overall agreement. The main difference is the shape and somewhat larger size of the area with high turbulent kinetic energy underneath the impeller for the simulation on the finest grid.

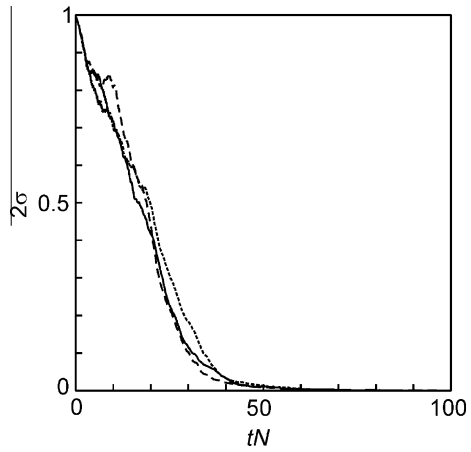

Fig. 13. Scalar standard deviation in the mid-baffle plane (σ) as a function of time; comparison between three different grids; short-dashed curve: the fine grid ($\Delta = T/330$), solid curve: intermediate grid, ($\Delta = T/240$), long-dashed curve: the coarser (default) grid ($\Delta = T/180$). Re = 12,000, Ri = 0.0625.

5. Summary, conclusions and outlook

Homogenization of initially segregated and stably stratified systems consisting of two miscible liquids with different density and the same kinematic viscosity by an axially pumping impeller was studied computationally. We restricted ourselves to flows with relatively low Reynolds numbers (in the range of 3000–12,000) to be able to solve the flow equations without explicitly modeling turbulence (in e.g. a large-eddy or RANS-based manner); this to avoid potential artifacts as a result of turbulence closure. This obviously limits the practical relevance of the presented work since most practical, industrial scale mixing systems operate at (much) higher Reynolds numbers.

The flow solution procedure was assessed in terms of its grid sensitivity which was considered important given our ambition to directly solve the flow, and specifically relevant since we needed to solve for the transport of a scalar that keeps track of the density (and thus buoyancy) field. The high Schmidt number (and therefore low diffusivity) makes the scalar field most sensitive with respect to resolution issues. A small but systematic impact of the grid

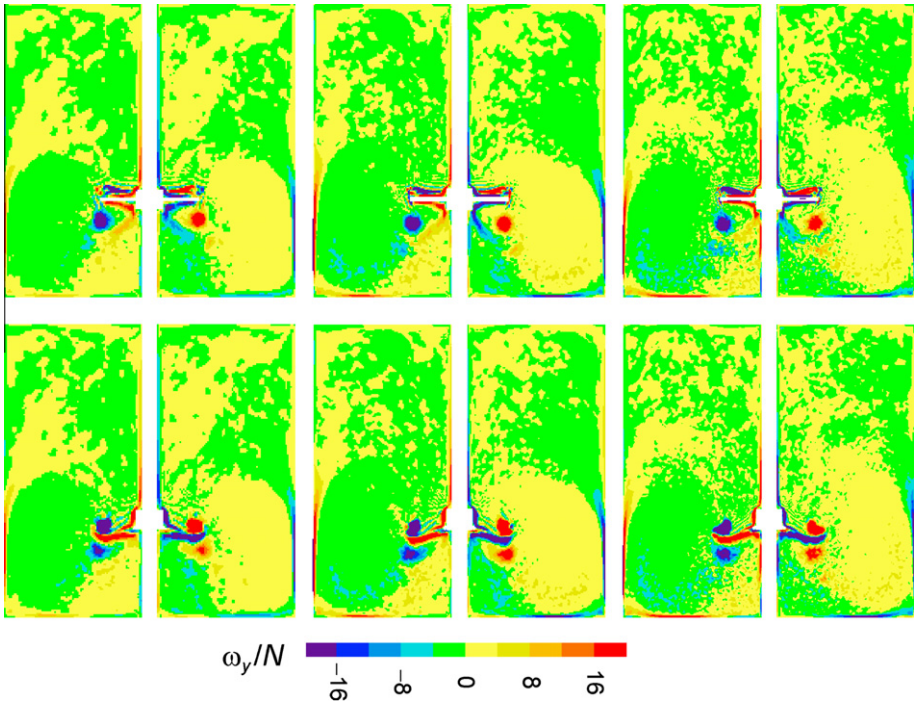

Fig. 14. Impeller-angle-resolved averaged vorticity component in the direction normal to the plane of view. Mid-baffle plane. Positive vorticity implies counter-clockwise rotation. Top row: the impeller blades cross the plane of view; bottom row: the impeller blades make an angle of 36° with the plane of view. From left to right: $\Delta = T/180$, $\Delta = T/240$, $\Delta = T/330$. Re = 12,000, Ri = 0.0625. (For interpretation to colours in this figure, the reader is referred to the web version of this paper.)

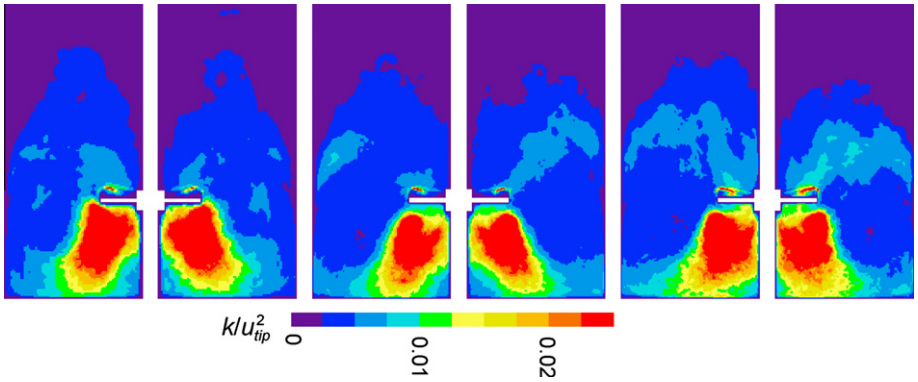

Fig. 15. Impeller-angle-resolved averaged turbulent kinetic energy in the mid-baffle plane. The impeller blades are in the plane of view. From left to right: $\Delta = T/180$, $\Delta = T/240$, $\Delta = T/330$. Re = 12,000, Ri = 0.0625. (For interpretation to colours in this figure, the reader is referred to the web version of this paper.)

spacing on the homogenization process was observed, specifically at the highest Reynolds number (12,000). We conclude that the resolution has had limited impact on the quantitative results as presented here. For identifying physical mechanisms and trends in our flow systems it is felt that the simulations were sufficiently resolved. The grid-refinement study also provides estimates as to how big numerical errors might be. Experimental work is needed to further assess accuracy.

Broadly speaking two flow regimes were identified. For "low" Richardson numbers the homogenization process is akin to the process with Ri = 0 and light and heavy liquid macro-mix through large, three-dimensional structures. For "larger" Richardson numbers the tank content maintains an identifiable, fairly horizontal interface with the light liquid above, and a denser liquid mixture below. The interface rises because of erosion: turbulence at the interface erodes light liquid that subsequently is drawn down by the impeller and well mixed in the volume below the interface. The boundary between the two flow regimes is not sharp. For the entire Reynolds number range considered the erosion regime could be observed for Ri = 0.5 and up. At Re = 3000 (the lowest Reynolds number) also at Ri = 0.25 erosion dominated homogenization. The rest of the cases did not show a clear and coherently rising interface. At the lowest Richardson number (0.03125) homogenization was roughly as fast as at Ri = 0.

An important purpose of presenting this work is to invite experimentalists to study similar flow systems in the lab. If necessary (or desired), two miscible liquids with different density *and* viscosity could be used for the experiments. As long as the viscosity (and density) as a function of the mixture composition is known, our simulation procedure should be able to represent the experiment.

References

[1] Fernando HJS. Turbulent mixing in stratified fluids. Annu Rev Fluid Mech 1991;23:455–93.
[2] Holford JM, Linden PF. Turbulent mixing in a stratified fluid. Dynam Atmos Oceans 1999;30:173–98.
[3] Maurer BD, Bolster DT, Linden PF. Intrusive gravity currents between two stably stratified fluids. J Fluid Mech 2010;647:53–69.
[4] Carruthers DJ, Hunt JCR. Velocity fluctuations near an interface between a turbulent region and a stably stratified layer. J Fluid Mech 1986;165:475–501.
[5] van de Vusse JG. Mixing by agitation of miscible liquids – part 1. Chem Eng Sci 1955;4:178–200.
[6] Ahmad SW, Latto B, Baird MH. Mixing of stratified liquids. Chem Eng Res Des 1985;63:157–67.
[7] Rielly CD, Pandit AB. The mixing of Newtonian liquids with large density and viscosity differences in mechanically agitated contactors. In: Proceedings of the 6th European Conference on Mixing, Pavia Italy; 1988. p. 69–77.
[8] Bouwmans I, Bakker A, van den Akker HEA. Blending liquids of differing viscosities and densities in stirred vessels. Chem Eng Res Des 1997;75:777–83.
[9] Derksen JJ, Prashant. Simulations of complex flow of thixotropic liquids. J Non-Newtonian Fluid Mech 2009;160:65–75.
[10] Frisch U, Hasslacher B, Pomeau Y. Lattice-gas automata for the Navier-Stokes Equation. Phys Rev Lett 1986;56:1505–8.
[11] Chen S, Doolen GD. Lattice Boltzmann method for fluid flows. Annu Rev Fluid Mech 1989;30:329–64.
[12] Yu DZ, Mei RW, Luo LS, Shyy W. Viscous flow computations with the method of lattice Boltzmann equation. Progr Aerosp Sci 2003;39:329–67.
[13] Succi S. The lattice Boltzmann equation for fluid dynamics and beyond. Oxford: Clarendon Press; 2001.
[14] Sukop MC, Thorne Jr DT. Lattice Boltzmann Modeling: An Introduction for Geoscientists and Engineers. Berlin: Springer; 2006.
[15] Somers JA. Direct simulation of fluid flow with cellular automata and the lattice-Boltzmann equation. Appl. Sci. Res. 1993;51:127–33.
[16] Goldstein D, Handler R, Sirovich L. Modeling a no-slip flow boundary with an external force field. J Comp Phys 1993;105:354–66.
[17] Derksen J, Van den Akker HEA. Large-eddy simulations on the flow driven by a Rushton turbine. AIChE J 1999;45:209–21.
[18] Hartmann H, Derksen JJ, Van den Akker HEA. Mixing times in a turbulent stirred tank by means of LES. AIChE J 2006;52:3696–706.
[19] Derksen JJ. Scalar mixing by granular particles. AIChE J 2008;54:1741–7.
[20] Sweby PK. High resolution schemes using flux limiters for hyperbolic conservation laws. SIAM J Numer Anal 1984;21:995–1011.
[21] Moin P, Mahesh K. Direct numerical simulation: a tool in turbulence research. Annu Rev Fluid Mech 1998;30:539–78.
[22] Eswaran V, Pope SB. An examination of forcing in direct numerical simulations of turbulence. Comput Fluids 1988;16:257–78.
[23] Grenville R, Ruszkowski S, Garred E. Blending of miscible liquids in the turbulent and transitional regimes. In: 15th NAMF Mixing Conf., Banff, Canada; 1995. p. 1–5.
[24] Bakker A, Myers KJ, Ward RW, Lee CK. The laminar and turbulent flow pattern of a pitched blade turbine. Trans IChemE 1996;74:485–91.
[25] Derksen J. Assessment of large eddy simulations for agitated flows. Trans. IChemE 2001;79:824–30.